

Investigation on Nd₂Fe₁₄B/ α -Fe nanocomposite magnets microalloyed with refractory elements

ZHANYONG WANG*, WENQING LIU^a, MINGLIN JIN, YANLI SUI^b

Department of Materials Science and Engineering, Shanghai Institute of Technology, Shanghai 201418

^aInstitute of Materials Science, Shanghai University, Shanghai 200072

^bState Key Laboratory for Advanced Metals and Materials, USTB, Beijing 100083

The microstructure and magnetic properties for Nd₂Fe₁₄B/ α -Fe nanocomposite magnets with Nb and Zr additions have been investigated. Zr-enriched clusters with 2~3 nm and $7 \times 10^6/\mu\text{m}^3$ in the size and number densities, respectively, have been found in as-spun amorphous ribbons. The concentration of Zr atom is about 30 at% for the clusters with total number of atoms higher than 40, which is about 9 times than its nominal composition and helpful to the grain refinement. With the addition of Zr and Nb elements, a fine and uniform microstructure with about 20~30 nm in grain size is obtained, which leads to the enhancement of the interaction coupling between the grains and improves the magnetic properties. The coercivity mechanism for nanocomposite magnets changes from nucleation mechanism for alloy without microalloyed elements to pinning mechanism for nanocomposites bearing with Nb and Zr.

(Received December 24, 2011; accepted June 6, 2012)

Keywords: Coercivity mechanism; Nd₂Fe₁₄B/ α -Fe; Crystallization; Elemental distribution

1. Introduction

Nanocomposite permanent magnets have received much considerable attention due to their potential properties after the first report of Nd₂Fe₁₄B/Fe₃B nanocomposite magnets [1]. The exchange coupling between magnetically hard and soft phases leads to the enhancement of remanence and coercivity owing to the nano grain size [2, 3]. The mean size of the soft grains should not exceed a small multiple of the wall width for the hard phase to ensure the effective coupling. And the size of hard phases also should be controlled in nano meters to ensure the enhancement of remanence. Therefore, the size, appearance and distribution of magnetically soft and hard phases are very important parameters to achieve good magnetic properties for nanocomposite permanent magnets.

Microalloying is the usual mean that is employed to modify the microstructure [4-11]. The small addition of refractory elements (such as Zr, Nb or V) has been reported as being useful in controlling the grain size of both the α -Fe and Nd₂Fe₁₄B phases for the precipitation of Nb-enriched [11], Zr-enriched and V-enriched phases at grain boundary [5]. These elements, distributing almost homogeneously in amorphous phase, have almost no solid solubility in magnetically soft or hard magnetic phases. Therefore, the redistribution of these elements is effective to control the precipitation of nanocrystalline phases. For the Nd₂Fe₁₄B/ α -Fe nanocomposite magnets with the addition of 5% Nb elements, the results of three-dimensional atom probe (3DAP) revealed that Nb-Fe-B intergranular phase with the ratio of Nb:Fe:B=1:1:1 existed at the boundary of grains,

suppressing the grain growth during crystallization process and resulting in high coercivity up to 1115kA/m [11]. The addition of Zr and Nb also refines the microstructure and improve the coercivity significantly for the fine microstructure and the precipitation of (Zr,Nb)Fe₂ phase at the interface of grains [10].

In this work, the microalloying of refractory elements, such as Nb and Zr additives, was investigated by applying the measurements of XRD, 3DAP and VSM.

2. Experimental

The ingots with the composition of (Nd_{0.9}Dy_{0.1})_{9.5}Fe₇₉Co₅B_{6.5} (sample A), (Nd_{0.9}Dy_{0.1})_{9.5}Fe_{75.5}Co₅Zr_{3.5}B_{6.5} (sample B) (Nd_{0.9}Dy_{0.1})_{9.5}Fe₇₈Co₅Nb₁B_{6.5} (sample C) and (Nd_{0.9}Dy_{0.1})_{9.5}Fe_{74.5}Co₅Nb₁Zr_{3.5}B_{6.5} (sample D) were prepared with pure Nd, Dy, Fe, Co, Nb, Zr as raw materials by non-consumable arc-melting under purified argon atmosphere. The ingots were put into quartz tube with an orifice diameter about 0.7 mm and melt-pun onto copper roll with wheel speed of 15 m/s. The obtained ribbons were annealed at 710 °C for 4 min in the vacuum of 2×10^{-3} Pa. The crystallization stage was ensured using differential thermal analysis (DTA) at a heating rate of 20 °C.min⁻¹. The structure of the as-spun and annealed ribbons was identified by X-ray diffraction instrument (D/max- γ B). 3DAP (Three-dimensional atom probe) instrument was employed to investigate the elemental distribution. As an instrument for investigating the microstructure of materials by analyzing atoms one by one, 3DAP can map out elemental distribution in a nanometric volume with near atomic resolution. Atom probe analysis is performed at a

tip temperature of about 65 K under an ultra-high vacuum condition ($<1 \times 10^{-8}$ Pa) with a pulse fraction (a ratio of pulse voltage to the static voltage) of 0.15 and a pulse repetition rate of 500 Hz. The magnetic properties of the ribbons were measured along the spun direction by VSM with maximum applied magnetic field of 1.8 T.

3. Results and discussion

Fig.1 shows the XRD patterns of as-spun ribbons for sample B, C and D. It is found that the as-spun ribbons mainly contain amorphous phase. Few weak diffraction peaks can be observed, revealing that a small amount of α -Fe and $\text{Nd}_2\text{Fe}_{14}\text{B}$ crystallization phases exists in the as-spun ribbons. The addition of refractory elements to the Fe-based alloy system was found to enhance its glass-forming ability (GFA) significantly [12-14]. Even the fracture surface similar to the polished mirror can be seen for the ingots prepared by non-consumable arc-melting.

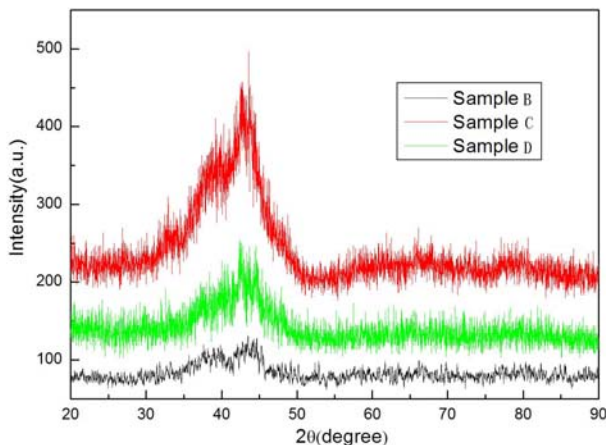


Fig.1 XRD patterns of as-spun ribbons for sample B, C and D.

In order to understand the as-spun ribbons in detail, the atomic concentration has been studied by 3DAP. A large number of clusters with different size and composed of micro-alloyed element and Fe element has been found. Fig.2 shows the element distribution in Zr-enriched clusters in as-spun ribbons for sample B. The size of Zr clusters is generally 2~3 nm with the cluster distribution density $7 \times 10^6/\mu\text{m}^3$. From all the elemental distribution maps in these clusters, a large amount of Fe atoms also can be seen in these clusters, but few for other elements. According to the composition of these clusters in Fig.2, the concentration of Zr and Fe elements are calculated according to the atom total number for each cluster, and quantitative results for the content of these two elements have been obtained. On the basis of the concentration and total atom number in each cluster, the curves about the relative content of Zr and Fe are shown in Fig.3. The less the total number of atoms in the cluster, the higher the concentration of Zr atoms is. For the clusters with total atomic number less than 20, the concentration of Zr atoms exceeds 50 at%. With the increase of the atoms in clusters, the composition of clusters becomes more and more stable.

The atomic concentration of Zr is about 30 at% for clusters with total number of atoms higher than 40, which is about 9 times than its nominal composition. Nb and Co-enriched clusters also have been found in the as-spun ribbons.

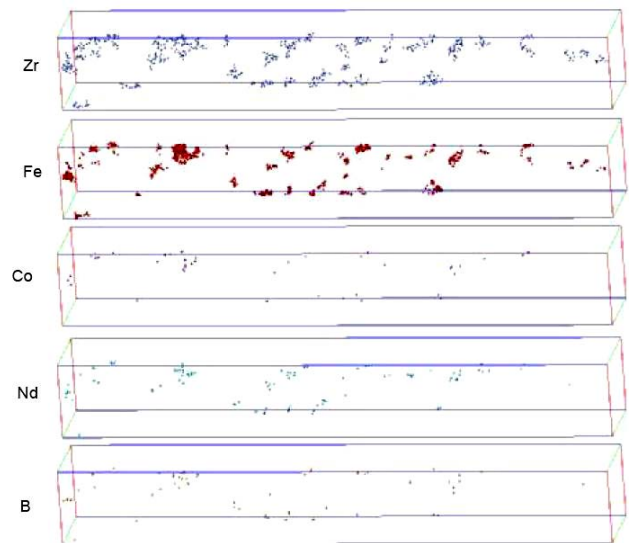


Fig.2 Elemental maps for all elements in Zr-enriched cluster ($8 \times 8 \times 62 \text{ nm}$).

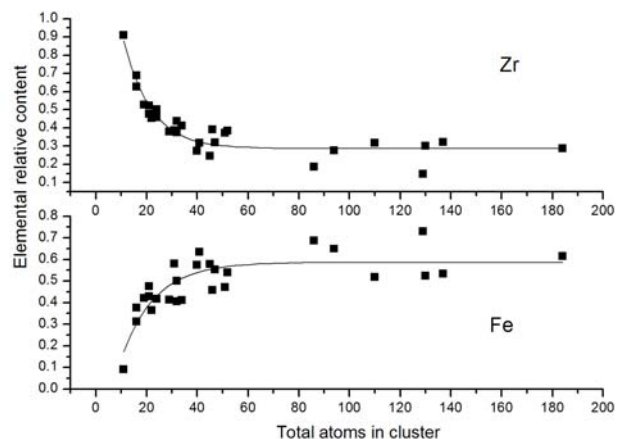


Fig.3 The relative content of Zr and Fe atoms in Zr-enriched clusters in as-spun ribbon for sample B.

These clusters have effects on the refinement of the crystallized microstructure similar as in Cu-enriched clusters [15]. As well known, Nb and Zr atoms have low or not solubility in hard-magnetic $\text{Nd}_2\text{Fe}_{14}\text{B}$ and soft-magnetic α -Fe phase, respectively. During the crystallization process of the as-spun ribbons, these atoms must diffuse to the boundary of these phases in order to result in the growth of $\text{Nd}_2\text{Fe}_{14}\text{B}$ or α -Fe phase. With the generation and growth of crystallized grains, the concentration of Nb and Zr elements at the front of the interface will constantly increase. Once the concentration of Nb and Zr elements is much higher, the energy needed to the grain boundary migration is also much higher and the rate of grain growth will decrease. So some researchers reported the existence of residual amorphous phase in annealed $\text{Nd}_2\text{Fe}_{14}\text{B}/\alpha$ -Fe nanocomposite ribbons [16-20]. On

the basis of above discussion, the high concentration of Zr- and Nb-enriched clusters could have significant effect on the grain refinement and the fine microstructure have been seen in the works [5,16~23].

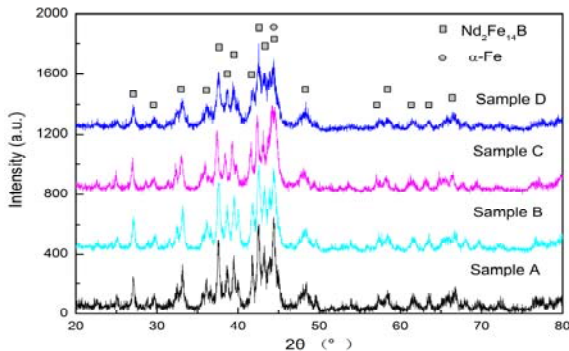
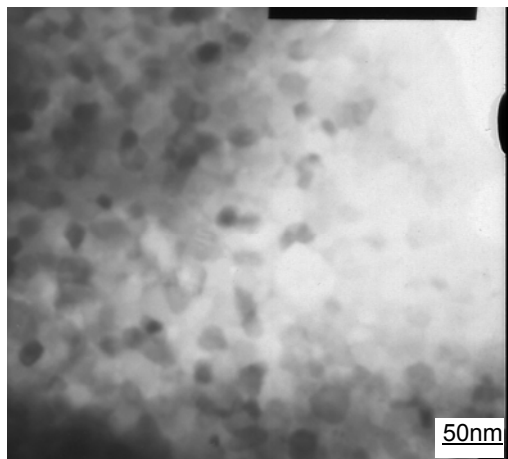
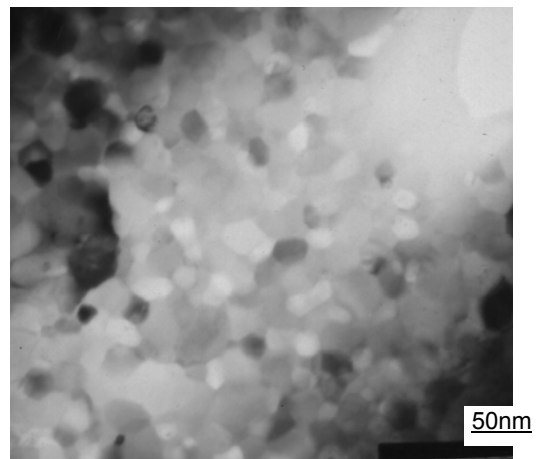


Fig.4 XRD patterns of sample A, B, C and D annealed at 710 °C for 4 minutes.

Fig. 4 shows the XRD patterns of sample A, B, C and D annealed at 710 °C for 4 minutes. The crystalline phases, α -Fe and Nd₂Fe₁₄B, are detected for all samples. Few differences can be found from the diffraction patterns of sample A and B. But for the samples C and D, the diffraction peaks become much weak, which reveals that fine nanocrystalline grains are obtained for the samples added with refractory elements. Fig. 5 shows microstructure of sample C and D ribbons annealed at 710 °C for 4 min. A fine and uniform microstructure with about 20~30 nm in grain size is obtained, which leads to the enhancement of the interaction coupling between the grains and improves the magnetic properties.

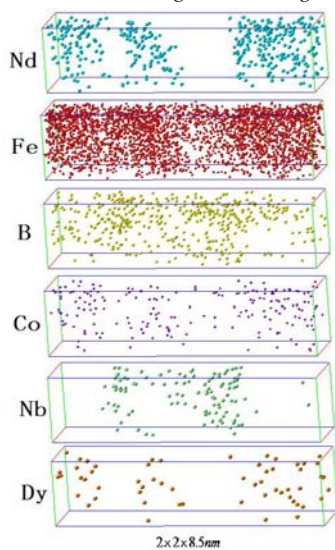


(a) Sample C

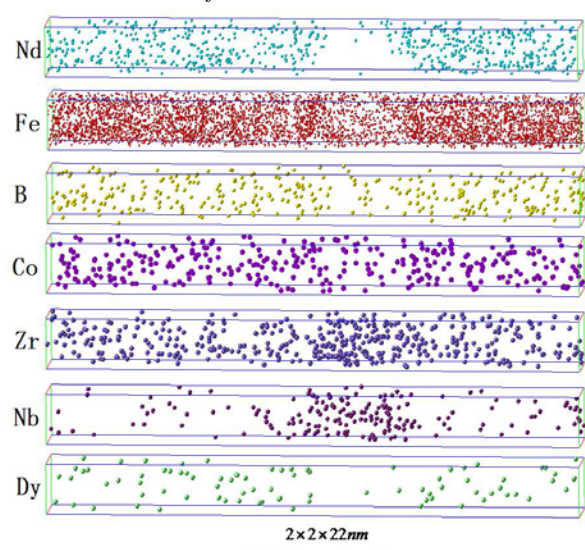


(b) Sample D

Fig.5 TEM imagines of sample C and D annealed at 710 °C for 4 minutes.



(a) Sample C



(b) Sample D

Fig.6 3DAP mappings of sample C and D annealed at 710 °C for 4 minutes.

3DAP were also applied to investigate the elemental distributions in annealed sample C and D to understand the formation of the fine microstructure, as shown in Fig.6. For sample C and D, Nb atoms, which don't dissolve in $\text{Nd}_2\text{Fe}_{14}\text{B}$ grains, precipitate at the boundary of $\text{Nd}_2\text{Fe}_{14}\text{B}$ grains. The elements Co and Dy have the same atomic distribution characters with Fe and Nd, respectively. The obvious difference between samples C and D is the atomic distribution of boron elements. For the sample C, boron atoms, combining with Nb and Fe atoms, enrich in the grain boundary of $\text{Nd}_2\text{Fe}_{14}\text{B}$ phase to form an amorphous phase Fe-Nb-B with higher amorphous stability [18]. However, for the samples D, boron atoms are poor at the grain boundary of $\text{Nd}_2\text{Fe}_{14}\text{B}$ phase. Another interesting phenomenon is that Zr atoms also enrich at the grain boundary of $\text{Nd}_2\text{Fe}_{14}\text{B}$ phase for sample D, although this element can be dissolved in $\text{Nd}_2\text{Fe}_{14}\text{B}$ grains and only slight enrichment can be found for samples with Zr single addition [22]. According to the concentration depth profiles, the concentration of Zr and Nb-enriched boundary phase is about 20 at%, 10 at% and 60 at% for Zr, Nb and Fe, respectively, similar with the composition of $(\text{Zr,Nb})\text{Fe}_2$ compound.

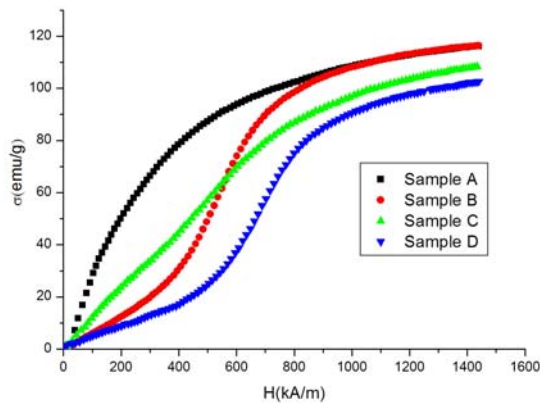


Fig. 7 The initial magnetization curves of annealed ribbons with different composition.

Fig.7 shows the initial magnetization curves of annealed ribbons with different composition. It can be seen that the addition of Zr and Nb has great effects on the initial magnetization. For the ribbons without alloy elements addition, the magnetization increases greatly with the increase of applied field at the initial magnetization stage. But for the ribbons with Nb and Zr elements added separately, the initial magnetization curves were changed from a steep increase to a gentle one, especially with Zr addition. The initial magnetization curve becomes much gentle with the co-addition of Zr and Nb elements. Nucleation and pinning mechanism are the main theory to explain the coercivity mechanism of permanent magnets [24]. Their hysteresis loops, especially the initial magnetization curves, present great difference in the shape, as shown in Fig.8 [25]. For nucleation mechanism, the coercivity is controlled by nucleation field

because of lack of defects, which lead to saturation magnetization under applied field with low intensity during initial magnetization. But for pinning mechanism, amounts of defects impede the migration of domain wall, which leads to the slow increase of magnetization curves at initial stage. Once the applied magnetic field exceeds the critical value, that is, the coercivity, the approach to saturation is much easier.

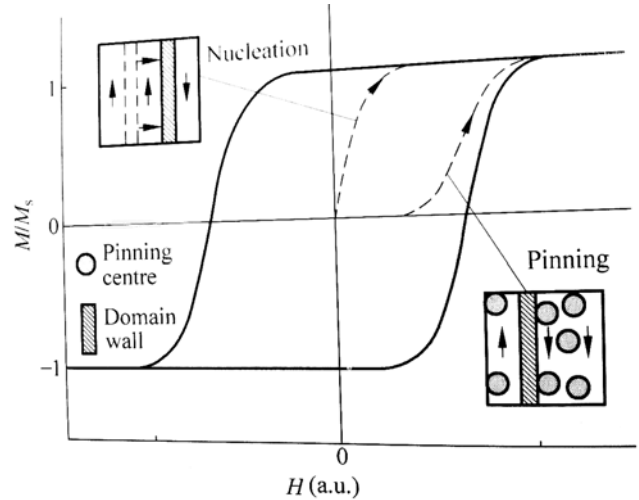


Fig. 8. The typical hysteresis loops for magnets with nucleation and pinning coercivity mechanism [25]

According to the typical initial magnetization curves in Fig.8, it can be concluded that with the addition of Zr and Nb, the coercivity mechanism for nanocomposite magnets change from Nucleation mechanism to pinning mechanism. As reported in other papers [10, 21, 26], amounts of phases enriched with Nb or Zr elements exist at the grain boundary. These grain boundary phases can pin the domain wall and hinder the reversal magnetization process, as mentioned grain boundary phase for Nd-Fe-B/Nd-Cu multilayer films [27]. According to the pinning mechanism reported by S.Z. Zhou [28], the magnetization reversal in $\text{R}_2\text{Fe}_{14}\text{B}/\alpha\text{-Fe}$ nanocomposite magnets undergoes the nucleation of reversal domain for soft-magnetic phase and the reversal domain migration from soft-magnetic phase to the hard-magnetic phase. The nucleation field of reversal domain for soft-magnetic phase, H_N , has great relations with the grain size of soft-magnetic phase, as shown in formula (1) [28].

$$H_N = \frac{2K_1^s(0)}{\mu_0 M_S} \frac{\delta_B^h}{\pi r_0} - N_{eff} M_S \quad (1)$$

Where r_0 , $K_1^s(0)$, M_S , μ_0 , δ_B^h and N_{eff} are radius, magnetic anisotropy constant, saturation magnetization of soft-magnetic phase, of soft-magnetic phase, vacuum permeability, domain thickness of hard-magnetic phase and demagnetization factor, respectively. So the grain refinement, especially the soft-magnetic grain [22], will improve the nucleation field of reversal domain, leading to

the enhancement of coercivity. In addition, the ultra-fine Nb-enriched and Zr-enriched phases in the annealed ribbons are soft-magnetic phase for their similar composition with FINEMET and NANOPERM alloy, which also has effects on the nucleation field and coercivity as well as α -Fe phase. As the planar magnetic inhomogeneities, the ultra-fine Nb-enriched and Zr-enriched phases with magnetic properties, different from the soft and hard magnetic phases, may act as rather effective pinning centres and be considered as strong planar pinning centres. As shown in formula (2), the pinning field is proportional to the volume density of pinning sites [29].

$$H_p = \frac{3\rho f^2}{4\pi\gamma M_s \mu_0} \quad (2)$$

where ρ is the volume density of pinning sites. The volume density of pinning sites increases with the formation of the phases enriched with refractory elements, which lead to a "strong" pinning and a high coercivity. The coercivity of annealed ribbons of sample A, B, C and D are 174 kA/m, 487 kA/m, 597 kA/m and 782 kA/m, respectively, as shown in Fig. 9.

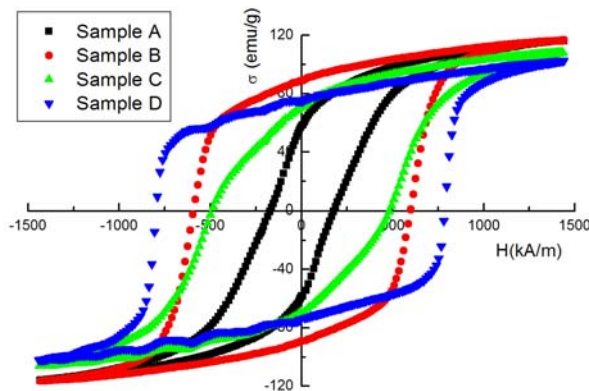


Fig. 9. The Hysteresis loop curves of annealed ribbons with different composition.

4. Conclusion

The addition of Nb and Zr elements to Nd₂Fe₁₄B/ α -Fe nanocomposite magnets has great effects on microstructure and coercivity. The as-spun ribbons for sample microalloyed show almost complete amorphous character. Zr-enriched clusters with size and distribution density in 2~3 nm and $7 \times 10^6/\mu\text{m}^3$, respectively, have been found in as-spun ribbons microalloyed. The atomic concentration of Zr is about 30 at% for clusters with total number of atoms higher than 40, being about 9 times than its nominal composition. The existence of these clusters is also helpful to the grain refinement due to their low or not solubility in hard-magnetic Nd₂Fe₁₄B and soft-magnetic

α -Fe phase. A fine and uniform microstructure with about 20~30 nm in grain size is obtained. The coercivity for samples with the addition of Zr and Nb has been improved greatly. The coercivity mechanism for nanocomposite magnets changes from nucleation mechanism for alloy without microalloyed elements to pinning mechanism for nanocomposites bearing with Nb and Zr.

Acknowledgements

This work was supported by Project of National Natural Science Foundation of China (51174030), the Shanghai Education Commission of PR China (10YZ181, 11CXY58 and J51504), Shanghai Science and Technology Committee of PR China (10ZR1429700) and State Key Lab of Advanced Metals Materials.

Reference

- [1] R Coehroon, D B De Mocchi and D De Waard, J. Magn. Magn. Mater. **80**, 101 (1989).
- [2] R. Skomski, J.M.D. Coey, Phys. Rev. B **48**, 15812 (1993).
- [3] T.Schrefl, R.Fischer, J.Fidler, H. Kronmuller, J. Appl. Phys. **76**, 7053 (1994).
- [4] Zhanyong Wang, Wenqing Liu, Yanli Sui, J. Optoelectron. Adv. Mater. **13**, 656 (2011).
- [5] K. Hono, Progress in Materials Science. **47**, 621 (2002).
- [6] G. C. Hadjipanayis, J. Magn. Magn. Mater., **200**, 373 (1999).
- [7] Choong Jin Yang, Jong Soo Han, Eon Byeung Park, Eng Chan Kim, J. Magn. Magn. Mater., **301**, 220 (2006).
- [8] S.Y. Zhang, H. Xu, J.S. Ni, H.L. Wang, X.L. Hou, Y.D. Dong, Physica B: Condensed Matter, **393**, 153 (2007).
- [9] W. Wang, J.S. Ni, H. Xu, B.X. Zhou, Q. Li. Physica B: Condensed Matter, **403**, 4186 (2008).
- [10] Z.Y. Wang, W.Q. Liu, B.X. Zhou, J.S. Ni, H. Xu, Proceedings of 19th International Workshop on Rare Earth Permanent Magnets & Their Applications, Beijing, 2006,183.
- [11] Z.Y. Wang, W.Q. Liu, B.X. Zhou, J.S. Ni, H. Xu, Y.Z. Fang, M.L. Jin, Physica B: Condensed Matter, **404**, 1321 (2009).
- [12] H.W. Chang, M.F. Shih, C.C. Hsieh, W.C. Chang, J. Alloys Compd., **484**, 143 (2009).
- [13] H.W. Chang, C.H. Chiu, C.W. Chang, C.H. Chen, W.C. Chang, Y.D. Yao, A.C. Sun, J. Alloys Compd., **407**, 53 (2006).
- [14] H. W. Chang, M. F. Shih, C. W. Chang, C. C. Hsieh, Y. K. Fang, W. C. Chang, A. C. Sun, J. Appl. Phys., **103**, 07E105 (2008).
- [15] Y.L. Sui, Z.Y. Wang, M.C. Zhang, S.Z. Zhou, J. Magn. Magn. Mater., **321**, 3974 (2009).
- [16] Y.Q. Wu, M.J. Kramer, Z. Chen, et al, IEEE Trans. Magn., **40**, 2886 (2004).

- [17] Y.Q. Wu, D.H. Ping, K. Hono, Inoue, IEEE Transactions on Magnetics, **35**, 3295 (1999).
- [18] Y.Q. Wu, D. H. Ping, K. Hono, M. Hamano, Inoue, J. Appl. Phys., **87**, 8658 (2000).
- [19] D.H.Ping, K.Hono, H.Kanekiyo, S.Hirosawa, Acta Metall. **47**, 4641 (1999).
- [20] K.Hono. Prog Mater Sci. **47**, 621 (2002).
- [21] Z.Y. Wang, W.Q. Liu, B.X. Zhou, J.S. Ni, H. Xu, Q. Li, Rare Metals, **27**, 299 (2008).
- [22] Y. Q. Wu, D. H. Ping, X. Y. Xiong, K. Hono, J. Appl. Phys., **91**, 8174 (2002).
- [23] C. Wang, M. Y. Lan, M. Yan, J Mater Sci. **45**, 5637 (2010).
- [24] E Burzo, Rep. Prog. Phys., **61**, 1099 (1998).
- [25] David J. Sellmyer, Yi Liu, D. Shindo, Handbook of advanced magnetic materials vol.1 [M], Beijing: Tsinghua University Press, 2005:22.
- [26] Z.Y. Wang, W.Q. Liu, Y.L. Sui, J. Optoelectron. Adv. Mater. **13**, 656 (2011).
- [27] S. Suzuki, Y.Hatayama, H.Iwama, T.Shima, IEEE Transactions on Magnetics. **47**, 2796 (2011).
- [28] S.Z. Zhou, Q.F. Dong, Supermagnets: Rare-earth & Iron System Permanent Magnet (in Chinese), Metallurgical Industry Press, Beijing, 2004.
- [29] E Burzo, Rep. Prog. Phys. **61**, 1099 (1998).

*Corresponding author: zhanyong.wang@vip.sina.com